Ninth Fuel and Combustion Conference of Iran
Feb. 8 - 10, 2022, Shiraz University, Shiraz, Iran
FCCI-2022-0081

Lattice Boltzmann simulation of forced convection in partial porous channel with application in exhaust gas recirculating (EGR) coolers

Alireza Khoshnood[1], Mehdi Maerefat[2*], Gholamreza Imani[3]
1 - Department of Mechanical Engineering, Tarbiat Modares University, Tehran, Iran. a.khoshnood@modares.ac.ir
2 - Department of Mechanical Engineering, Tarbiat Modares University, Tehran, Iran. maerefat@modares.ac.ir
3 - Department of Mechanical Engineering, Persian Gulf University, Bushehr, Iran. g.r.imani@pgu.ac.ir
*Corresponding author

Abstract
Diesel engines are one of the main sources of NO_x emission, which occurs due to the high flame temperature in such engines. Using an exhaust gas recirculation (EGR) system is one of the methods introduced to reduce the flame temperature and consequently the NO_x emission in diesel engines. The EGR gas is usually passed through a cooler for its temperature to be reduced before reentering the cylinder to increase the efficiency of an EGR system. Because of the high-temperature gradients in the cooler, the particles fouling on the cooler's surface are very likely to occur which disrupts the system's performance. Using the EGR system helps to reduce NO_x, but instead, it causes the increment of a particular matter and soot particle according to the incomplete combustion. These produced particles deposit on the cooler walls and create a porous layer that disrupts the system's hydrodynamic and heat transfer performance. In this paper, a partial porous channel is considered as a simple single-passage EGR cooler. The lattice Boltzmann method (LBM) is used to numerically investigate the effect of different Darcy-number (0.1, 0.01, 0.001) and various dimensionless blockage ratios by the porous layer ($e = 0.2, 0.4, 0.6$) on hydrodynamic and heat transfer performance.
Keywords: NO_x emission, diesel engines, exhaust gas recirculation cooler, partial porous channel, lattice Boltzmann method.

Introduction

Particular matters (PM) such as CO_2 and NO_x are emissions caused by diesel engines. These emissions are believed to significantly contribute to global warming and acid rain. NO_x is more harmful to the environment than other counterparts, and diesel engines are the greatest source of NO_x emission because of the high flame temperature [1, 2]. One of the best and widely used ways for reducing NO_x is to return part of the exhaust gas to the intake. As can be seen in Figure 1, this is usually carried out via a heat exchanger (EGR cooler) to increase the heat capacity of the recirculated gas [3, 4]. The EGR can reduce the flame temperature and NO_x emission with four separate effects, namely the additive mass effect, dilution oxygen effect, thermal effect, and chemical effect [5, 6].

Using the EGR system is helpful to reduce the NO_x emission, but it also causes the PM to increase. Ladommatos et al. [7] showed that the EGR could reduce about 50 percent of NO_x emission of a diesel engine but increased the PM products by 50 percent. Dicky et al. [8]reported that adding an EGR system to diesel engines can cause PM-products even to increase 1000 times greater than diesel without an EGR system. Fouling of this PM product is a significant problem because they build porous layers in the cooler of this system which can be problematic in terms of efficiency reduction.

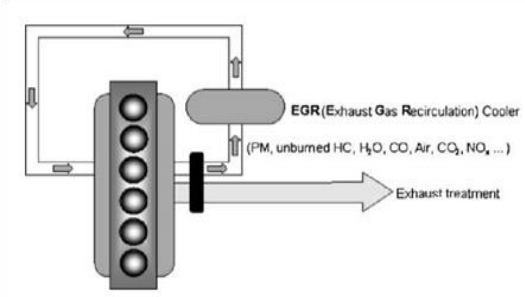

Figure 1 EGR scheme[2]

The main reason behind the fouling of PM and consequently building up the porous layer is the thermophoresis force applied to hot particles, which pushes them towards the cold surface [9]. Abraham et al. [1] indicated that the thermophoresis force is the most influential force affecting particle fouling in EGR cooler systems because of the high-temperature gradients.
Numerous studies have been done to investigate this phenomenon and its effects on the performance of EGR coolers. For example, Malayeri et al. [10] experimentally investigated the effect of gas velocity magnitude on the fouling layer thickness and reported that increasing velocity causes the fouling layer thickness to reduce. Teng et al. [11] reported that the increased deposit porous layer thickness on the heat transfer surfaces lead to a decrease in the effectiveness of the EGR cooler and an increase in the flow resistance. Abraham et al. [12] suggested a 1-D model for predicting and calculating EGR cooler fouling amount, and they investigated the influence of porous layer on parameters such as effectiveness, mass deposition, and pressure drop. The results showed good agreement with the experimental data.

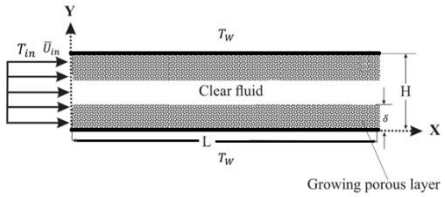

Figure 2 The partial porous channel model

Kuang-Kuan et al. [13] developed a 1-D CFD fouling model for predicting the thermal effectiveness reduction of real EGR coolers. They showed that the fouling layer that was formed on the EGR cooler surface degraded the heat transfer performance and increased pressure drop across the cooler and, in extreme cases, could even completely plug the cooler.

According to the above literature survey, there are few works that numerically simulated fluid flow and heat transfer in an EGR cooler. In this study, a single-passage EGR cooler is assumed as a partial porous channel. In this study, the effect of different porous layer blockage ratios (e = 0.2, 0.4, 0.6) and various Darcy numbers (0.1, 0.01, 0.001) have been investigated by the lattice Boltzmann method (LBM). In the present study, the EGR rate is considered to be low, so the laminar flow is assumed. Furthermore, the constant wall temperature condition is considered at the channel walls.

2. The model definition

As shown in Figure 2, the LBM simulation of the fluid flow and heat transfer inside a parallel plate channel with partial porous layers on the lower and upper walls is considered for this study. In fact, the partial porous channel is assumed as the single-passage of the EGR cooler, and both walls have a constant temperature. The fluid enters the channel with the initial constant temperature and fully developed velocity. The laminar flow with a low Reynolds number is considered in this study which resembles a low EGR rate in the EGR cooler system. According to Figure 3, because of the deposited layer's asymptotic behavior in real life EGR coolers, the fouling layer thickness reaches a final constant thickness [14, 15], after which the porous layer thickness remains unchanged similar to the geometry considered here.

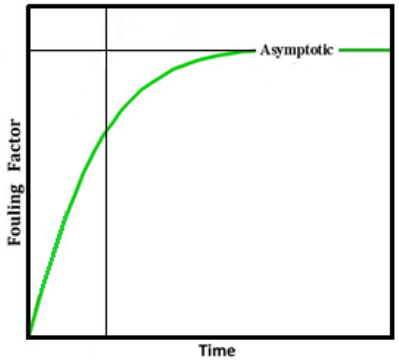

Figure 3 The asymptotic behaviour of fouling layer [16]

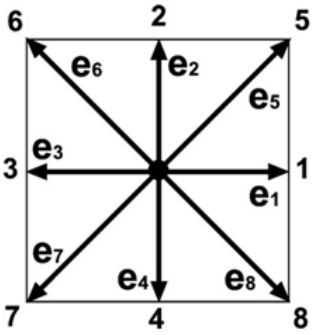

Figure 4 the LBM D2Q9 model[17]

3. Mathematical model

This section presents the LBM governing equations of the fluid flow and heat transfer in a channel partially filled with a porous medium.

3.1. The hydrodynamic equations

The LBM model has been used for simulating flow in saturated porous media. Equation (1) represents the evolution of the density distribution function:

$$f_\alpha(x + e_\alpha \delta t, t + \delta t) - f_\alpha(x,t) = \frac{f_\alpha^{eq}(x,t) - f_\alpha(x,t)}{\tau_v} + \delta t F_\alpha \quad (1)$$

In equation (1) , f_α is the density distribution function, f_α^{eq} is the density equilibrium distribution function given by equation (2), δt is time step and F_α is the discrete body force in lattice direction α and defined in equation (3):

$$f_\alpha^{eq} = \omega_\alpha \rho \left[1 + \frac{e_\alpha \cdot u}{C_s^2} + \frac{(e_\alpha \cdot u)^2}{2C_s^4} - \frac{u \cdot u}{C_s^2}\right] \quad (2)$$

$$F_\alpha = \omega_\alpha \rho \left(1 - \frac{1}{2\tau_v}\right)\left[\frac{e_\alpha \cdot F}{C_s^2} + \frac{uF : e_\alpha e_\alpha}{C_s^4} - \frac{u \cdot F}{C_s^2}\right] \quad (3)$$

In equations (2) and (3) C_s is the speed of sound, and it has relation by streaming speed that defined as ($C = \delta x/\delta t, \delta x$ is space step) which can be written as ($C_s = C/\sqrt{3}$). For the model, Streaming speed has been 1 ($C = 1$), so the speed of sound is defined by ($C_s = 1/\sqrt{3}$).

τ_v is dimensionless velocity field relaxation time used in equations (1) and (3) and is considered to be 0.91

$$\tau_v = \left(\frac{3\nu_f}{\delta t}\right) + (0.5) \quad (4)$$

The LBM D2Q9 model (two dimensions and nine velocity directions) has been used for simulation. Therefore, in Figure 4, the α index denotes nine discrete speed directions ($\alpha = 0, \dots, 8$) and e_α is particle velocity vectors, and ν_f is kinematic viscosity.

e_α is the discrete velocity and ω_α is the weighted coefficient given as follows:

$$e_\alpha = \begin{cases} 0, & \alpha = 0 \\ \cos[(\alpha-1)\pi/4)], \sin[(\alpha-1)\pi/4)]C, & \alpha = 1,2,3,4 \\ \sqrt{2}\cos[(\alpha-1)\pi/4)], \sin[(\alpha-1)\pi/4)]C, & \alpha = 5,6,7,8 \end{cases} \quad (5)$$

$$\omega_\alpha = \begin{cases} 4/9, & \alpha = 0 \\ 1/9, & \alpha = 1,2,3,4 \\ 1/36, & \alpha = 5,6,7,8 \end{cases} \quad (6)$$

The macroscopic quantities can be written as:

$$\rho = \sum_\alpha f_\alpha \quad (7)$$

$$u = \sum_\alpha (f_\alpha e_\alpha + \frac{\delta t}{2}\rho F)/\rho \quad (8)$$

where ρ is the fluid density and u is fluid velocity.
The fluid velocity in porous media can be calculated from equation (9):

$$u = V/(d_0 + \sqrt{d_0^2 + d_1|V|}) \quad (9)$$

where V is the temporal velocity vector $\left(V = \frac{\sum_\alpha f_\alpha e_\alpha}{\rho}\right)$ and d_0, d_1 are two factors determined as:

$$d_0 = \frac{1}{2}\left(1 + \varepsilon\frac{\delta t}{2}\frac{\nu_f}{K}\right) \quad (10)$$

$$d_1 = \varepsilon^2\frac{\delta t}{2}\frac{F_\varepsilon}{\sqrt{K}} \quad (11)$$

where ε is the porosity of the porous media and F_ε is the geometrical function defined as:

$$F_\varepsilon = \frac{1.75}{\sqrt{150\varepsilon^3}} \quad (12)$$

The Navier-Stokes equation for incompressible fluid flow can be reconstructed by applying a Chapman-Enskog expansion in low Mach number limits as follows:

$$\nabla \cdot u = 0 \quad (13)$$

$$\frac{\partial u}{\partial t} + (u \cdot \nabla)(u) = -\frac{1}{\rho}\nabla(p) + \nu_e \nabla^2 u + F \quad (14)$$

In equations (13) and (14), ρ is the fluid density, u is the fluid velocity, p is pressure ($p = \rho C_s^2$), ν_e is the effective kinematic viscosity $\nu_e = C_s^2(\tau_\nu - 0.5)\delta t$, and F is total body force which is calculated from equation (15):

$$F = -\frac{\varepsilon\nu}{K}u - \frac{\varepsilon^2 F_\varepsilon}{\sqrt{K}}|u|u \quad (15)$$

where ν is the shear viscosity of the fluid, and K is the permeability of porous medium determined by:

$$K = \frac{Da}{(2H)^2} \quad (16)$$

In equation (16) Da is the dimensionless permeability (Darcy-Number), and H is the width of the channel, as shown in Figure 1.

3.2. Energy equations

The LBGK model with local thermal equilibrium (LTE) assumption between the solid and liquid phases is used for simulating the heat transfer in porous media. Thus, the evolution equation for the energy distribution function is given by:

$$g_\alpha(x + e_\alpha\delta t, t + \delta t) - g_\alpha(x,t) = \frac{g_\alpha^{eq}(x,t) - g_\alpha(x,t)}{\tau_t} \quad (17)$$

where τ_t is temperature dimensionless relaxation time ($\tau_t = ((\tau_\nu - 0.5)/\mathrm{pr}) + 0.5$), $g_\alpha(x,t)$ is energy distribution function, and $g_\alpha^{eq}(x,t)$ is equilibrium distribution function defined by equation (18):

$$g_\alpha^{eq} = \omega_\alpha T\left[1 + \frac{e_\alpha \cdot u}{C_s^2}\right] \quad (18)$$

Where T is volume-averaged fluid temperature.
The macroscopic volume-averaged energy equation with LTE assumption can be derived by applying a Chapman-Enskog expansion as shown in equation (20):

$$\frac{\partial T}{\partial t} + u \cdot \nabla \mathrm{T} = \nabla \cdot (\alpha_e \nabla T) \quad (20)$$

where α_e is effective thermal diffusivity defined as $\alpha_e = C_s^2(\tau_t - 0.5)\delta t$.

4. Boundary conditions

The Hydrodynamic and energy boundary conditions used in this study are presented as follows [17]:

4.1. Hydrodynamic boundary conditions:

Inlet:

The Zuo-He method [18] has been used to apply the fully-developed condition for the inlet boundary

Outlet:

$$f_\alpha(N_x, y) = 2f_\alpha(N_x - 1, y) - f_\alpha(N_x - 2, y), \qquad \alpha = 3,6,7 \quad (21)$$

The second order extrapolation method is used for determining unknown distribution functions [18]:
Where N_x and N_y are the number of grids in x and y directions, respectively.

Solid Wall:

No-slip conditions have been assumed for a wall using the Zuo-He method [18].

4.2. Energy boundary conditions:

Inlet boundary and solid walls:

The D'Orazio method [19] is used for inlet and wall temperature conditions. In this method, the unknown energy distribution functions are considered to be the equilibrium populations with a slip temperature T^{eq}.

For the inlet boundary:

$$\begin{aligned} g_{1=} &\frac{1}{9}T^{eq}\left[1 + \frac{3}{c^2}u\right] \\ g_{5=} &\frac{1}{36}T^{eq}\left[1 + \frac{3}{c^2}(u+v)\right] \\ g_{8=} &\frac{1}{36}T^{eq}\left[1 + \frac{3}{c^2}(u-v)\right] \end{aligned} \quad (22)$$

$$T^{eq} = \frac{6(T_{in} - T_P)}{1 + \frac{3}{C^2}u} \quad (23)$$

Where T_{in} is the macroscopic temperature at the inlet and T_P is the sum of known energy distribution populations at the inlet.

For upper wall:

$$\begin{aligned} g_{4=} &\frac{1}{9}T^{eq} \\ g_{7=} &\frac{1}{36}T^{eq} \\ g_{8=} &\frac{1}{36}T^{eq} \end{aligned} \quad (24)$$

For lower wall:

$$\begin{aligned} g_{2=} &\frac{1}{9}T^{eq} \\ g_{5=} &\frac{1}{36}T^{eq} \end{aligned} \quad (25)$$

$$g_{6=}\frac{1}{36}T^{eq}$$
$$T^{eq}=6(T_w-T_P) \quad (26)$$

Where T_w is the macroscopic temperature of lower and upper walls and T_P is the sum of known energy distribution populations for each case.

Outlet boundary condition:

The second order extrapolation method is applied for the outlet condition as the following:

$$g_\alpha(N_x,y)=2g_\alpha(N_x-1,y)-g_\alpha(N_x-2,y), \quad \alpha=3,6,7 \quad (27)$$

5. Numerical simulation

The LBM-LBGK method is used for simulating the fluid flow and heat transfer in a partial porous channel, as illustrated in Figure 1. In this study, the low EGR rate is considered, so the Reynolds number defined by equation (28) has been assumed to be 50 [20]. The effect of different Darcy Numbers (0.1, 0.01, 0.001) and non-dimensional blockage ratios on the hydrodynamic and the local Nusselt-number on a lower wall defined in equation (29) is investigated, the Prandtl-number that is shown in equation (30) is considered to be 0.74. According to experimental data related to EGR coolers, the porosity of the deposited layer (ε) is considered to be 0.9 [15], the inlet gas temperature (T_{in}) of 600K is taken and the walls are in the constant temperature of 353K (T_w). The length of the channel is assumed five times bigger than the width (see in Figure 1). The dimensionless blockage ratio of the porous layer can be calculated from equation (31):

$$Re=\frac{\rho u(2H)}{\nu} \quad (28)$$

$$Nu=\frac{h(2H)}{k} \quad (29)$$

$$Pr=\frac{\nu}{\alpha_f} \quad (30)$$

$$e=\frac{2\delta}{H} \quad (31)$$

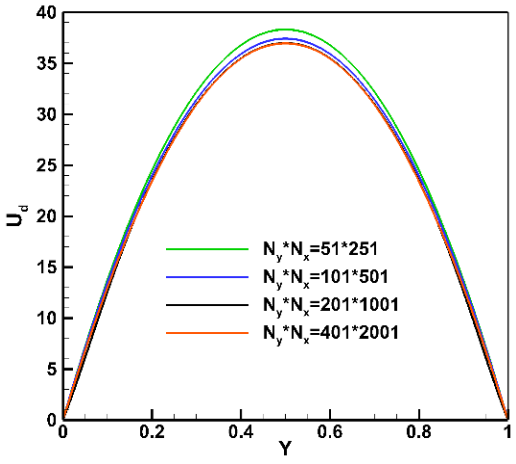

Figure 5 grid independence

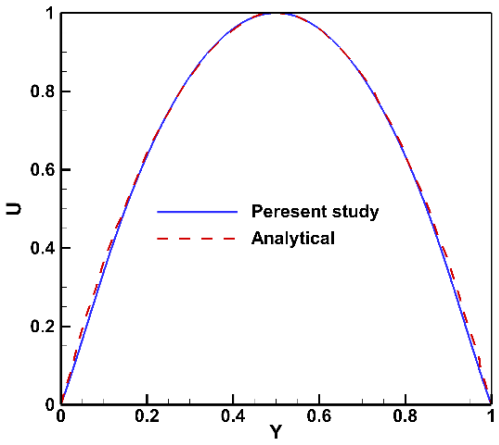

Figure 6 dimensionless velocity empty channel validation

In equations (28-31) H is the width of the channel, k is the thermal conductivity of the fluid, α_f is the fluid thermal diffusivity and δ is porous thickness on one wall (see Figure 1).

5.1. Grid independence

In Figure 5, the results of the grid independence for the hydrodynamic problem in an empty (i.e., clean) channel are presented. Figure 5 shows the comparison of the non-dimensional velocity (U_d) (defined in equation (32)) versus dimensionless width (Y) (defined in equation (33)) for different grids sizing. As can be seen in Figure 5, the results are mesh independent for the mesh size 201× 1005.

$$U_d=\frac{uH}{\nu_f} \quad (32)$$

$$Y=\frac{y}{H} \quad (33)$$

In equation (33) y is dimensional width, and Y is dimensionless width.

6. Results and Discussion

6.1. Validation

For validating the numerical method, the non-dimensional velocity (U) is compared with the analytical one for the clean channel, which can be seen in Figure 6. the local Nusselt number for the clean channel is compared to the analytical one versus the non-dimensional longitudinal coordinate ($X=(x/2H)/(\mathrm{Re}\cdot\mathrm{Pr})$) [17]. As seen in Figure 7, the fully-developed Nusselt number of 7.56 is predicted in this study, while the analytical one is reported to be 7.54 [21]. Hence, the results show good agreement with analytical results.

6.2. Profiles of dimensionless velocity and Nusselt-number

The effect of different Darcy numbers on the velocity profiles and different non-dimensional blockage ratios versus dimensionless width is shown in Figures 8 (a), (b) and (c).The results indicated that by increasing the Darcy number, the fluid velocity in the porous material region increased, but in the clear region, the fluid velocity decreased. Generally, the mean velocity in the clear region is much higher than that in the porous region (see Figure 8).

The local Nusselt numbers profiles versus dimensionless longitudinal coordinate (X) are presented in Figures 9 (a), (b) and (c). As shown in Figure 9 (a), (b), and (c), the effect of blockage ratio on the Nusselt number is more evident in cases with lower Darcy numbers. It is also shown in Figure 8 that the dimensionless velocity in the clear region is increased by increasing the porous layer thickness and non-dimensional blockage ratio. Therefore, as the Darcy number increases, the porous layer effects vanish, and the partial porous duct behaves as a clear duct. However, for the small value of Darcy numbers, the porous layer acts as an impermeable medium (see Figure 8).

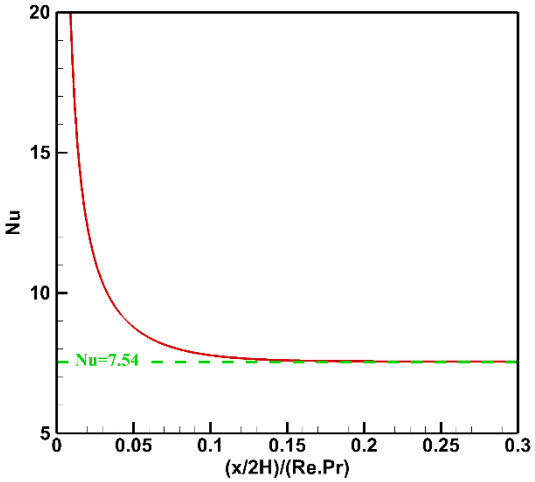

Figure 7 Local Nusselt number on the lower wall

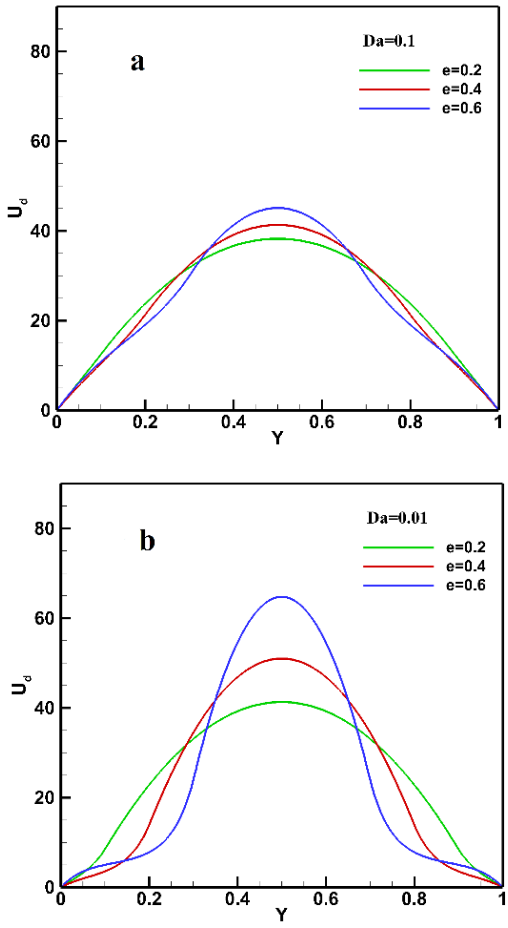

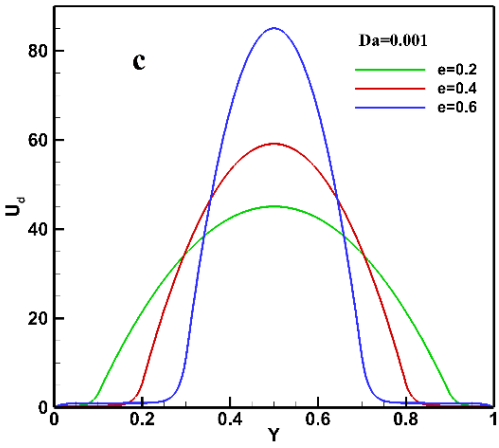

Figure 8 dimensionless velocity profile for different blockage ratio with porous layer, and different Darcy-number, a) Da=0.1, b) Da=0.01, c) Da=0.001

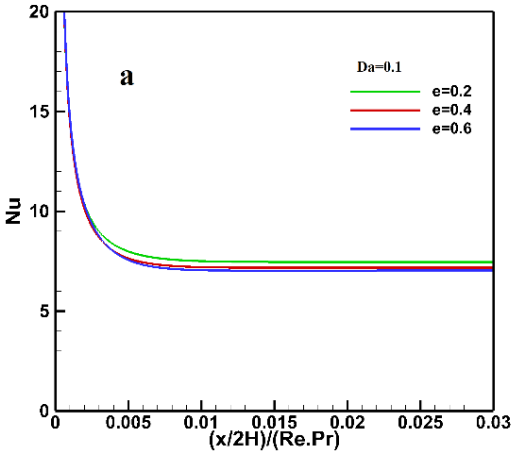

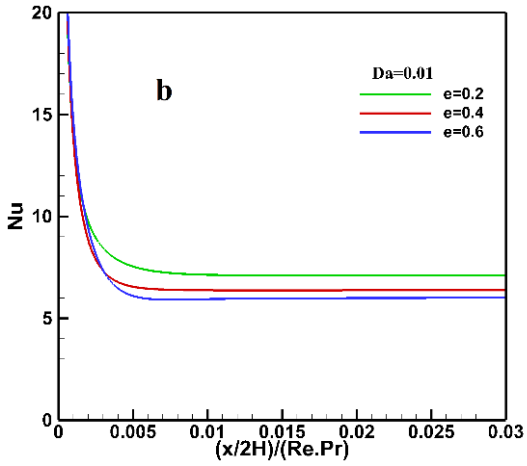

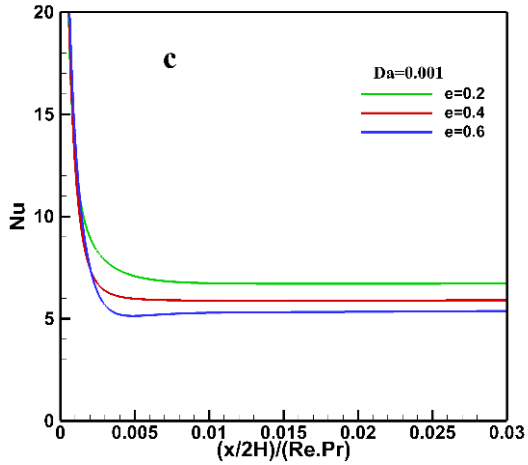

Figure 9 local Nusselt-number on wall for different blockage ratio by porous layer, and different Darcy-number, a) Da=0.1, b) Da=0.01, c) Da=0.001

The embedded porous layer at the boundary of the channel causes more fluid to flow in the core of the channel, and therefore, the velocity in the porous layer decreases (see Figure 8). Hence, the contiguity of the fluid flow with the solid wall reduces, and subsequently, the Nusselt number decreases. So, for the lower Darcy number, the decay rate of Nusselt-number is more prominent (see Figure9).

6.3. The effect of different blockage ratios by the porous layer and various Darcy-number on fully-developed Nusselt-number

According to Figure 10, by increasing the Darcy number, the amount of reduction in the local Nusselt number caused by the porous layer decreases. The decay rate of the Nusselt number from $e = 0.2$ to 0.4 for all the Darcy numbers is more than $e = 0.4$ to 0.6. Figure 11 shows that for Darcy number equal to 0.1, this decay trend continues until a particular thickness in which the Nusselt number is minimized. As presented in Figure 12, a further increase in the porous thickness decreases the gap between the clear fluid and the porous region. Thus, the fluid does not prefer to flow in the clear region. Hence, more fluid flows through the porous layer and the Nusselt number increases.

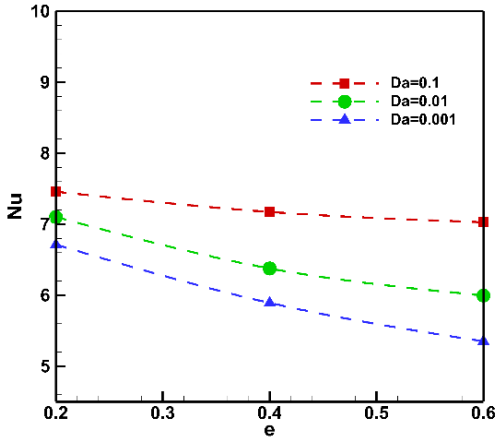

Figure 10 fully-developed Nusselt number on the lower wall for different dimensionless blockage ratios and Darcy numbers

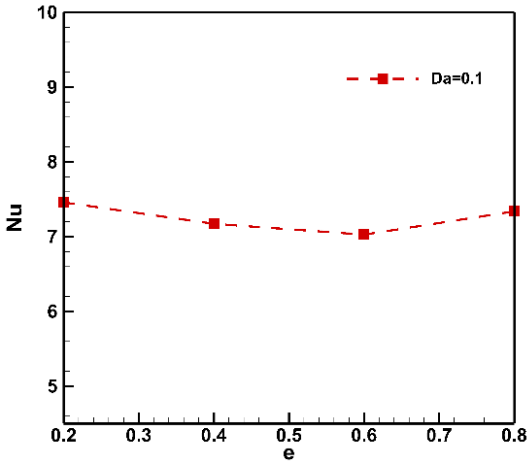

Figure 11 fully-developed Nusselt number on the lower wall for different dimensionless blockage ratio at Darcy number 0.1

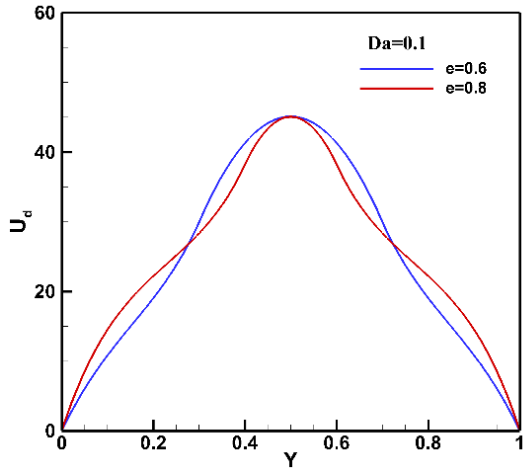

Figure 12 dimensionless velocity profile for dimensionless blockage ratio 0.6 and 0.8 at Darcy number 0.1

Conclusion

The LBM method is used for numerical simulation of the fluid flow and heat transfer in a parallel plate channel partially filled with porous media as a simple geometry of a single-pass EGR cooler model in the asymptotic fouling regime. Energy equations in both clear and porous regions have been solved. The effect of the different dimensionless blockage ratios by porous layer and various Darcy numbers on the local and fully-developed Nusselt numbers and velocity profiles has been investigated. The results showed that by increasing the Darcy number, the effect of dimensionless blockage ratios on the Nusselt and velocity profiles evolution decreases. The effect of 0.2, 0.4, and 0.6 blockage ratios for the different Darcy Numbers 0.1, 0.01, and 0.001 have been investigated. The results showed that when the porous layer non-dimensional thickness is increased from 0.2 to 0.6, the fully developed Nusselt number is decreased. However, it is shown that the rate of Nusselt number reduction was more pronounced for 0.2 to 0.4. Even in Darcy number of 0.1, the Nusselt number and velocity profile for blockage ratio 0.4 and 0.6 are almost the same. For Darcy number of 0.1 in blockage ratio of 0.8, the Nusselt number

increases because the gap between the clear fluid and the porous region decreases, and flow prefers to penetrate through the porous material (see Figure 11 and Figure 12).

List of Symbols

C	stream speed
C_p	heat capacity
C_s	speed of sound
d_0	porous factor
d_1	porous factor
Da	Darcy-number
dx	space step
e	dimensionless blockage ratio
e_α	discrete velocity
F	total body force
f_α	velocity distribution function
f_α^{eq}	equilibrium velocity distribution function
F_ε	geometrical function
g_α	temperature distribution function
g_α^{eq}	equilibrium temperature distribution function
H	width of the channel
h	heat convection coefficient
K	permeability
L	length of the channel
Nu	Nusselt
N_x	number of grids in width
N_y	number of grids in length
Re	Reynolds-number
T	volume-averaged fluid temperature
T_{in}	inlet temperature
T_p	summation of known temperature distribution
T_w	wall temperature
	Function after streaming
T^{eq}	unknown equilibrium volume-averaged fluid temperature
u	fluid velocity vector
$\bar{u}_{in}$	average inlet fluid velocity
V	temporal velocity vector
X	non-dimensional longitudinal coordinate
y	dimensional width
Y	dimensionless width

Greek:

α_e	effective thermal diffusivity
α_f	fluid thermal diffusivity
δ	porous layer thickness on one wall
δ_t	time step
ε	porosity
ν_e	effective kinematic viscosity
ν_f	kinematic viscosity
ρ	fluid density
σ	volumetric heat capacity
τ_t	the non-dimensional relaxation time of temperature distribution function
τ_v	non-dimensional relaxation time of density distribution function
ω_α	weighted coefficient

References

[1]Abarham, M., et al., *Review of soot deposition and removal mechanisms in EGR coolers.* SAE International Journal of Fuels and Lubricants, 2010. **3**(1): p. 690-704.

[2]Abd-Elhady, M.S., M.R. Malayeri, and H. Müller-Steinhagen, *Fouling problems in exhaust gas recirculation coolers in the automotive industry.* Heat Transfer Engineering, 2011. **32**(3-4): p. 248-257.

[3]Pourrezaei, M., M. Malayeri, and K. Hooman, *Thermal performance and mechanisms of soot deposition in foam structured exhaust gas recirculation coolers.* International Journal of Thermal Sciences, 2019. **146**: p. 106108.

[4]Hoard, J., et al., *Diesel EGR cooler fouling.* SAE International Journal of Engines, 2009. **1**(1): p. 1234-1250.

[5]Punitharani, K. and V. Parameshwaran, *Effect of exhaust gas recirculation on performance of a diesel engine fueled with waste plastic oil/diesel blends.* Strojnícky časopis-Journal of Mechanical Engineering, 2017. **67**(2): p. 91-100.

[6]Sobh, A.J., *The Aspects of Fouling on the Performance of Diesel Exhaust Gas Recirculation Coolers.* 2011.

[7]Ladommatos, N., et al., *Effects of EGR on heat release in diesel combustion*, 1998, SAE Technical Paper.

[8]Ismail, B.I.A., *The heat transfer and the soot deposition characteristics in diesel engine exhaust gas recirculation system cooling devices*, 2004.

[9]A.khoshnood, M.Maerefat. GH.Imani, *Introduction of various types of diesel engine exhaust gas recirculation systems and importance of thermophoresis force in particle deposition*, in *The 29th Annual International Conference of the Iranian Association of Mechanical Engineers*2021: Tehran, Iran.

[10]Malayeri, M.R., et al., *Deposition of nanosized soot particles in various EGR coolers under thermophoretic and isothermal conditions.* Heat Transfer Engineering, 2013. **34**(8-9): p. 665-673.

[11]Teng, H. and M. Barnard, *Physicochemical characteristics of soot deposits in EGR coolers*, 2010, SAE Technical Paper.

[12]Abarham, M., et al., *Numerical modeling and experimental investigations of EGR cooler fouling in a diesel engine*, 2009, SAE Technical Paper.

[13]Kuan, C.-K., et al., *An EGR cooler fouling model: Experimental correlation and model uses.* SAE International Journal of Engines, 2017. **10**(2): p. 541-549.

[14]de Pinho, S.R.G.G., *Fouling of Exhaust Gas Recirculation Coolers.* 2017.

[15]Salvi, A.A., et al., *Optical and Infrared In-Situ Measurements of EGR Cooler Fouling.* SAE Technical Paper, 2013(2013-01): p. 1289.

[16]Paz, C., et al., *Development of a predictive CFD fouling model for diesel engine exhaust gas systems.* Heat Transfer Engineering, 2013. **34**(8-9): p. 674-682.

[17]Shokouhmand, H., F. Jam, and M. Salimpour, *Simulation of laminar flow and convective heat transfer in conduits filled with porous media using Lattice Boltzmann Method.* International Communications in Heat and Mass Transfer, 2009. **36**(4): p. 378-384.

[18]Sukop, M., *DT Thorne, Jr. Lattice Boltzmann Modeling Lattice Boltzmann Modeling*. 2006: Springer.

[19]D'Orazio, A. and S. Succi. *Boundary conditions for thermal lattice Boltzmann simulations*. in *International Conference on Computational Science*. 2003. Springer.

[20]Bika, A.S., et al., *Characterization of soot deposition and particle nucleation in exhaust gas recirculation coolers.* Aerosol Science and Technology, 2012. **46**(12): p. 1328-1336.

[21]Kays, W. and M. Crawford, *Convective Heat and Mass Transfer McGraw-Hill.* New York, 1993: p. 255-282.